

Reconstruction of annular bi-layered media in cylindrical waveguide section

Anders Eriksson ^{*} Truls Martin Larsen [†] Larisa Beilina [‡]

Abstract

A radial transverse resonance model for two cylindrical concentric layers with different complex dielectric constants is presented. An inverse problem with four unknowns - 3 physical material parameters and one dimensional dielectric layer thickness parameter- is solved by employing TE₁₁₀ and TE₂₁₀ modes with different radial field distribution. First a Newton-Raphson algorithm is used to solve a least square problem with a Lorentzian function (as resonance model and "measured" data generator). Then found resonance frequencies and quality factors are used in a second inverse Newton-Raphson algorithm that solves four transverse resonance equations in order to get four unknown parameters. The use of TE₁₁₀ and TE₂₁₀ models offers one dimensional radial tomographic capability. An open ended coax quarter-wave resonator is added to the sensor topology, and the effect on the convergence is investigated.

Keywords: reconstruction of material parameters in a waveguide, transverse resonance model, open ended coax resonator, least squares problem.

1 Introduction

Extraction of material parameters and/or dimensions based on distributed resonator measurements has been around for decades. Characterization of distributed microwave resonators dielectric material from resonance frequency and quality factor measurements is found in [1]. A comparison of inverse methods for extracting resonant frequency and quality factor is given in [2]. Typically, the dielectric filling of the resonators is homogeneous, but there are not really any restrictions for allowing inhomogeneous dielectric filling. In this work, two annular concentric cylindrical layers which are enclosed in a finite conductive metallic pipe, each with a frequency dependent dielectric constant, is modelled and four unknown physical parameters are found using a transverse resonance radial model, alone as well as with additional open ended coax quarter wave resonators. The possible applications are characterization of metallic pipes with annular flow, or characterization of optical fibers and similar geometries.

2 Notations

The complex dielectric constant can be expressed as:

$$(1) \quad \varepsilon = \varepsilon_0 \varepsilon_r = \varepsilon_0 (\varepsilon_{Re} - i \varepsilon_{Im}) = \varepsilon_0 \left(\varepsilon_{Re} - i \frac{\sigma}{\omega} \right),$$

^{*}FMC Technologies, Kongsberg Norway, e-mail: danandersgustav@fmcti.com

[†]FMC Technologies, Kongsberg Norway, e-mail: trulsmartin.larsen@fmcti.com

[‡]Department of Mathematical Sciences, Chalmers University of Technology and University of Gothenburg, SE-412 96 Gothenburg, Sweden, e-mail: larisa@chalmers.se

where ε_0 is the electric permittivity in vacuum, ε_r is the dimensionless relative electric permittivity, ε_{Re} , ε_{Im} are the real and imaginary parts of the relative permittivity for an arbitrary material, respectively, σ is the electrical conductivity, and ω is angular frequency. The equation (1) applies to imperfect metal with finite conductivity as well as to the dielectric materials under investigation.

Measurement Parameter	Description
h	Thickness of liquid layer - liquid having arbitrary mixture ratio (Water Void Fraction) of condensate and saline water.
R_{WLR}	Water Liquid Ratio (WLR) - water fraction in liquid.
R_{DGR}	Droplet Gas Ratio (DGR) - ratio of liquid immersed in droplet form in gas continuous volume (note that WLR and Salinity is the same in liquid film as well as in droplets).
s	Salinity - salt concentration in water.

Table 1: Parameters to be determined.

2.1 Modelling of permittivity of emulsions and saline water

In this work, there are 4 different media (3 different media) - salt (NaCl), hydrocarbon gas, Water (H_2O) and oil. No water vapor is assumed in the calculations. Bruggemans model for emulsion permittivity [9, 10] is used. This model is applied for saline water mixed with oil as well as for liquid droplets in gas. For the latter, Bruggemans model is used twice - first for water mixed with oil in liquid droplets, and then again to calculate the effective permittivity of liquid droplets in gas.

Several models for effective complex permittivity of metal powders in insulating dielectrics (e.g. teflon) are studied in [10], and one conclusion is that Bruggeman models are relatively accurate for predicting real part of permittivity while the well-known Maxwell-Garnett models have higher accuracies for the imaginary part. This is relevant for the case of an oil continuous regime with water content of high salinity - where the electrically conducting saline water droplets are comparable to electrically conducting metal powder. Gadani's model [8] for saline water is used to describe a complex permittivity of the saline water. The complex permittivity is a function of salinity (s), temperature (T) and frequency (f) in this model.

Thus, by applying these permittivity models with corresponding fractions for each medium (assuming that the known chemical substances are presented but with unknown ratios), the parameters are reduced in this case to 4 unknowns, while in the case of using directly a frequency-dependent complex permittivity for the liquid, and another frequency-dependent complex permittivity for the gas, 4 unknowns would be left to solve just for one frequency point along with the liquid thickness, rendering 5 unknown. Then from these permittivities, the WLR and droplet fraction in gas would have to be found.

For simplicity, the dielectric constants for gas and oil are set to be 1.7 and 2.0, respectively.

2.2 Direct Problem

A full wave RF resonance model using transverse resonance method is very computationally efficient and compact (equation wise). It can model infinite long cylindrical pipe or waveguide,

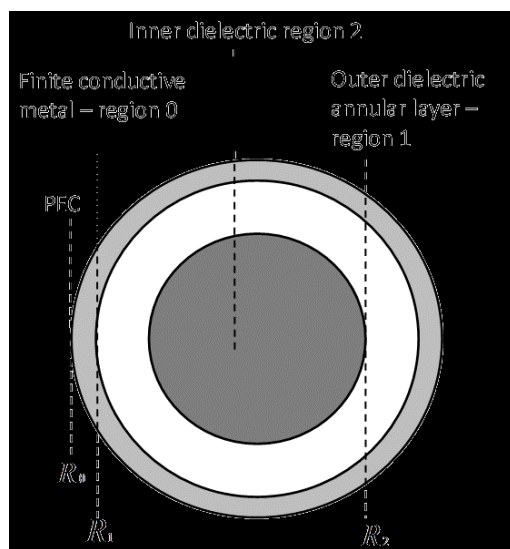


Figure 1: Cross-section of the annular waveguide section.

Parameter	Description
ε_r	Relative electric permittivity
ε_0	Electric permittivity in vacuum
ε	$\varepsilon_0 \cdot \varepsilon_r$
μ_r	Relative magnetic permeability
μ_0	Magnetic permeability in vacuum
μ	$\mu_r \cdot \mu_0$
ω	Angular frequency
ω_0	Angular resonant frequency, $2\pi f_0$.
f_0	Resonant frequency
Q_0	Unloaded quality factor
TE_{mnl}	Transverse electric mode with angular index m, radial index n, and longitudinal index z.
TM	Transverse magnetic mode.
$H_m^{(1)}(r)$	Hankel function of the first kind.
$H_m^{(2)}(r)$	Hankel function of the second kind.
$H_m^{(1)'}(r)$	Derivative of Hankel function of the first kind.
$H_m^{(2)'}(r)$	Derivative of Hankel function of the second kind.
$J_m(r)$	Bessel function.
f_{Re}	Real part of the function f.
f_{Im}	Imaginary part of the function f.
S_{11}	Reflection coefficient
S_{21}	Transmission coefficient

Table 2: Fundamental notations.

filled with arbitrary concentric layers. Ideal boundary conditions in z-direction may also be modeled.

Full wave models for open ended coax are typically more complex and require much more computational effort. In order to be used in a real time application, a parameterized fast model without any numerical integration would typically be needed.

2.2.1 Radial transverse resonance method

For circular cylindrical waveguides composed of at least 2 different dielectrics ($\varepsilon_{r1} \neq \varepsilon_{r2}$ and/or $\mu_{r1} \neq \mu_{r2}$) supports in general no pure TM and TE modes except for symmetrical cases when angular index $m = 0$ (TE_{0nl} and TM_{0nl}). In this case when angular index $m = 0$, the characteristic equation from the determinant of a 4x4 matrix (matrix derived from matching tangential magnetic and electric fields H_z, H_θ, E_z and E_θ for the 2 layer dielectrics case) can be factorized such that the equation can be factorized to a product of a TM and TE characteristic equation [5]. However, the elements in the 4x4 matrix (for two layered circular cylindrical waveguide) containing angular index m also contains longitudinal wave number k_z . At radial resonance (i.e. cut-off frequency), the longitudinal wave number $k_z = 0$, and thus the same matrix elements that becomes zero when $m = 0$ also becomes zero when even for longitudinal index $k_z = 0$. Thus, TM and TE radial resonances (where $k_z = 0$) for any angular index may be accommodated.

The quality factor of a TE or TM mode will in theory be decreased by leaking waves, e.g. surface waves. Typically, for transmission based resonator measurements, the external coupling to the resonator is relatively weak - thus, $|S_{11}|^2 + |S_{21}|^2 \approx 1$, indicating that the unloaded quality

factor (stored energy to dissipated energy ratio) is dominant. In practice, this is realized by relatively small antennas/probes such that mainly fringing antenna field is exciting the resonance. Under such conditions, external quality factor is relatively large compared to the unloaded quality factor, rendering unloaded Q (intrinsic desired resonator Q) equal to the loaded Q (measured Q).

The radial propagation constant is defined as

$$(2) \quad \beta_\rho^2 = k^2 - k_z^2,$$

where

$$(3) \quad k^2 = \omega^2 \mu_0 \mu_r \varepsilon_0 \varepsilon_r$$

is free space wave number and k_z is the longitudinal wavenumber, which includes a complex resonance frequency $\omega_0 = \omega_{0Re} + i\omega_{0Im}$ at resonance ($\omega \rightarrow \omega_0$). The Q -factor of the composed multi-concentric layered structure is computed as in [4]

$$(4) \quad Q_0 = \frac{\omega_{0Re}}{2\omega_{0Im}}.$$

Setting the radial propagation constant $\nu := \beta_\rho = \sqrt{k^2 - k_z^2}$, and assuming that there is no variation in z-direction (i.e. a pure radial resonance) renders the propagation constant as $\nu = \omega\sqrt{\mu\varepsilon}$ with $\mu\varepsilon = \mu_0\mu_r\varepsilon_0\varepsilon_r$.

Let us now move to establish a suitable radial impedance transformation model. Since the wave impedance is anisotropic in radial direction [5], the reflection coefficient must be derived accordingly. Let Y_C^+ and Y_C^- be the anisotropic admittances in outward and inward directions, respectively. We define the reflection at the load as $\Gamma = V^-/V^+$, where V^- , V^+ are reflected and incident voltage at load Z_L , respectively, the outgoing current as $I^+ = Y_C^+ V^+$ and the reflected current as $I^- = Y_C^- V^-$. Finally, $V^+ + V^- = V_L$, $I^+ - I^- = I_L$ renders a reflection coefficient at the load impedance Z_L :

$$(5) \quad \Gamma_L = \frac{Z_C^-(Z_L - Z_C^+)}{Z_C^+(Z_L + Z_C^-)},$$

where characteristic anisotropic impedance $Z_C^- = (Y_C^-)^{-1}$ and $Z_C^+ = (Y_C^+)^{-1}$.

It is noticed that equation (5) simplifies to:

$$(6) \quad \Gamma_L = \frac{Z_L - Z_C}{Z_L + Z_C}$$

for isotropic characteristic impedance.

2.2.2 Impedance Transformation

For notations used in this and following sections, we refer to table 2. For cylindrical TE wave the characteristic impedance for a radial outgoing TE wave [5] is given by the formula:

$$(7) \quad Z_{Cout} = \frac{E_\phi}{H_z} = i \frac{\omega \mu H_m^{(2)'}(\nu r)}{\nu H_m^{(2)}(\nu r)}.$$

The characteristic impedance for a radial incoming wave is given by the formula:

$$(8) \quad Z_{Cin} = \frac{E_\phi}{H_z} = -i \frac{\omega \mu H_m^{(1)'}(\nu r)}{\nu H_m^{(1)}(\nu r)}.$$

With the voltage ratio $\frac{V_0^-}{V_0^+}$ at the load at r_0 given by the formula:

$$(9) \quad \frac{V_0^-}{V_0^+} = \frac{H_m^{(2)'}(\nu r) Z_{Cin}(r_0) (Z_L - Z_{Cout}(r_0))}{H_m^{(1)'}(\nu r) Z_{Cout}(r_0) (Z_L + Z_{Cin}(r_0))}$$

the transformed load impedance from r_0 to r becomes

$$(10) \quad Z_{out}(r) = \frac{Z_{Cin}(1 + \Gamma(r))}{\frac{Z_{Cin}}{Z_{Cout}} - \Gamma(r)} = \frac{Z_{Cin}(1 + \frac{V_0^- H_m^{(1)'(\nu r)}}{V_0^+ H_m^{(2)'(\nu r)}})}{\frac{Z_{Cin}}{Z_{Cout}} - \frac{V_0^- H_m^{(1)'(\nu r)}}{V_0^+ H_m^{(2)'(\nu r)}}}.$$

We simplify last expression to get numerically efficient formulas which are used in computations by introducing notations

$$(11) \quad \begin{aligned} F_1(x) &= Z_L H_m^{(2)}(x) - B H_m^{(2)'(x)}, \\ F_2(x) &= B H_m^{(1)'(x)} - Z_L H_m^{(1)}(x), \end{aligned}$$

where the load Z_L is given at radius r_0 (for $r_0 > r$). Then (10) can be rewritten as

$$(12) \quad Z_{out}(r) = \frac{B H_m^{(1)'(\nu r)} F_1(\nu r_0) + H_m^{(2)'(\nu r)} F_2(\nu r_0)}{H_m^{(1)}(\nu r) F_1(\nu r_0) + H_m^{(2)}(\nu r) F_2(\nu r_0)},$$

with $B = \frac{i\omega\mu}{\nu} = i\sqrt{\frac{\mu}{\epsilon}}$. We scale this expression with exponential function in order to handle finite metal conductivity:

$$(13) \quad Z_{out}(r) = \frac{B e^{2i\nu(r-r_0)} H_m^{(1)'(\nu r)} F_1(\nu r_0) + H_m^{(2)'(\nu r)} F_2(\nu r_0)}{e^{2i\nu(r-r_0)} H_m^{(1)}(\nu r) F_1(\nu r_0) + H_m^{(2)}(\nu r) F_2(\nu r_0)}.$$

The inward input impedance into the innermost region is given by the formula:

$$(14) \quad Z_{in}(r) = B \frac{J_m'(\nu r)}{J_m(\nu r)}.$$

Resonance condition is fulfilled when $Z_{in}(r_{bound}) + Z_{out}(r_{bound}) = 0$ for both real and imaginary parts. The resonance condition can be calculated at any r_{bound} inside the circular cylindrical region. In this work $r_{bound} = R_2$ (see Figure 1).

2.2.3 Impedance Transformation For cylindrical TM wave

We follow the same steps as for TE wave, except that the characteristic impedance for an outgoing wave is given by the formula:

$$(15) \quad Z_{Cout} = -\frac{E_z}{H_\phi} = -\frac{i\nu H_m^{(2)}(\nu r)}{\epsilon k H_m^{(2)'(\nu r)}}.$$

The characteristic impedance for an incoming wave can be computed as

$$(16) \quad Z_{Cin} = -\frac{E_z}{H_\phi} = \frac{i\nu H_m^{(1)}(\nu r)}{\epsilon k H_m^{(1)'(\nu r)}}.$$

Introducing notations

$$(17) \quad \begin{aligned} F_3(x) &= Z_L H_m^{(1)'}(x) - A H_m^{(1)}(x), \\ F_4(x) &= Z_L H_m^{(2)'}(x) - A H_m^{(2)}(x), \end{aligned}$$

we scale the obtained expression for Z_{out} with exponential function in order to handle finite metal conductivity:

$$(18) \quad Z_{out}(r) = \frac{A H_m^{(2)}(\nu r) F_3(\nu r_0) - e^{2iv(r-r_0)} H_m^{(1)}(\nu r) F_4(\nu r_0)}{H_m^{(2)'}(\nu r) F_3(\nu r_0) - e^{2iv(r-r_0)} H_m^{(1)'}(\nu r) F_4(\nu r_0)},$$

where $A = \frac{i\nu}{\varepsilon k} = i\sqrt{\frac{\mu}{\varepsilon}}$.

The inward input impedance into the innermost region can be computed simply as:

$$(19) \quad Z_{in}(r) = A \frac{J_m(\nu r)}{J_m'(\nu r)}.$$

A test code (the same code as used for generating electromagnetic fields in [6]) based on a spectral domain Greens function for cylindrical geometry [7] was compared to the transverse resonance method for both TE and TM modes for verification (with $k_z = 0$: where an excitation current in z-direction renders TM modes, and an excitation in transverse angular ϕ direction, renders TE modes).

2.2.4 TE110 and TE210 Mode Field Distribution for 1-Dimensional Radial Tomography

In the case when angular index $m \gg 1$, then the electric field is dominant near resonator radius (see the equivalent field distribution for parallel plate TM disc resonators [3]). Even TE210 mode has electric field significantly more confined near pipe radius compared to TE110, which have a more homogeneous electric field distribution. This can be exploited tomographically, since TE210 mode field pattern penetrates less radially inwards than compared to the TE110 mode. Thus, the TE210 mode is more sensitive to the presence of an outer concentric dielectric layer than compared to the TE110 mode.

Having the quality factor and resonance frequency for each TE110 and TE210 mode, a set of four unknown material and dimensional parameters can in theory be extracted using the same transverse resonance technique described previously.

2.2.5 Open Ended Coax Quarter-wave Resonator Probe

An open ended coax quarter-wave resonator exposed to pipe can serve as an additional measurement probe. If dimensioned properly (i.e. with suitable coax diameters a and b), its penetration depth may be shorter than even the TE210 mode. The open-ended coax resonator gives typically a quality factor and resonance frequency for low-loss exposed media ("open-circuit" type load) as well as high loss exposed media ("short-circuit"). For the latter case, the frequency shift is negligible, while amplitude changes decreases with increased electric media loss. An intermediate region between low and high loss renders a rather "arbitrary" wave-form, where the open end of coax sees more of "matched load" impedance. Thus, in the low-loss region, the resonator is "open-ended quarter wave", while in high-loss region, it is half-wave type resonator (high electrical loss imply higher electrical conductive load).

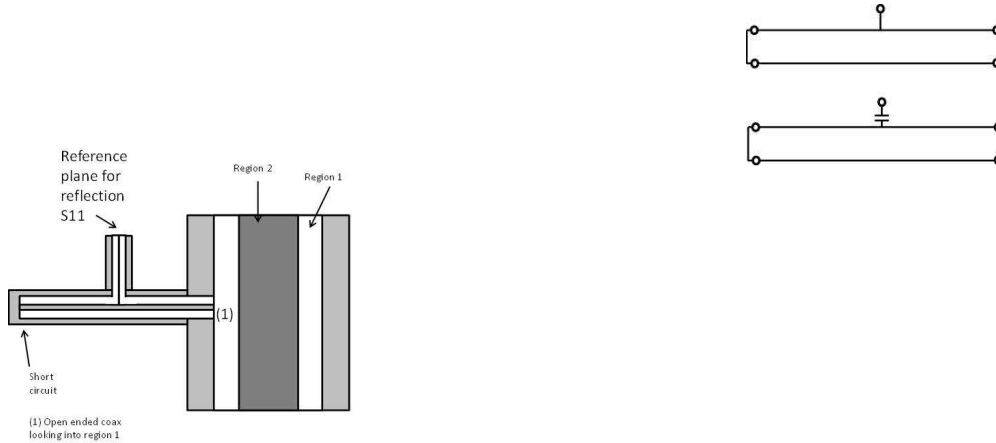


Figure 2: At the left is open ended galvanic coupled quarter-wave coaxial resonator connected flush to waveguide pipe section. At the right is schematic circuits of galvanic and capacitive coupled quarter-wave resonators

In this work, the direct magnitude reflection response is minimized with respect to the model of open ended coax and its quarter-wave transmission-line circuitry - without any intermediate resonance frequency and Q -factor calculations.

We apply the full-wave Hankel transform based model in [11]. If the pipe diameter is significantly larger than the coax outer diameter b , the planar ground plane model in [11] is assumed still to be valid. It is noted that the abrupt discontinuity from the coax section into a grounded plane excites higher order terms apart from the fundamental incident coax TEM mode. In [11], these higher modes are TM modes with only radial variations due to the angular symmetry. If the coax diameter b increases relative to the pipe diameter D , the angular variations of the basis functions/higher modes would be stronger - however not estimated to be as large as the radial higher mode excitations.

A compromise in accuracy would be to assume an incident ideal TEM wave, and matching the tangential electric and magnetic fields at the curved open ended coax- pipe interface using a spectral domain approach [7], and using basis functions/modes with angular dependency (in local open-ended coax coordinate system).

For suitable coax dimensions a , b , a third characteristic penetration depth (smaller than TE₂₁₀) can be obtained, and thus, one can replace one of the four transverse resonance equations with an equation for the open-ended coax resonator.

As model for input impedance Z_{liq} , a full-wave model of [11] is employed; using fundamental TEM mode, and two lowest TM modes as basis functions, and the input impedance is calculated

from the obtained TEM reflection coefficient. The reflection coefficient S_{11} at reference plane in figure 2(a) is obtained by standard impedance transformations.

Typically, for low-salinity exposed media, the response in S_{11} are resonance poles shifting down in frequency with increased water content of the exposed media. For a "high" saline media, the quarter-wave resonator turns in effect into a half-wave resonator due to the high conductive saline media that is exposed to the open coax end. In this high salinity water continuous regime, the frequency shift is very weak, while amplitude changes are still significant - even for salinities above 12%, but the amplitude change starts to decrease with increasing salinity in this high salinity region.

2.2.6 Coupling to the open-ended quarter wave coax resonator

By probing the resonator in the middle of the coax instead of at the left end, separation of the resonance frequencies is narrowed for the same physical resonator length. Practically (if not also theoretically) is impossible to select an optimal coupling to a quarter-wave open ended coax loaded with media, while having a large range for the imaginary part as well as real part (with salinities from 0 up to 25% the imaginary part of saline water changes with several orders of magnitude). The magnitude of the response ($mag(S_{11})$) will not have a monotonic change in amplitude as permittivity real and imaginary parts change.

Experimentally we have found that using a pair of resonators - see lower figure 2 (one that is simply galvanic coupled, and the another one is capacitive coupled, in this work a coupling capacitance of 10 pF), a better sensitivity in amplitude and frequency shift is achieved. We should note that a pair of capacitive and galvanic coupled resonators cannot render more information than a phase and magnitude reflection measurement directly at the open end of the coax, but rather, they (resonator pair) transform the complex reflection data to resonance type response, so that the benefit of both amplitude change as well as frequency shift can be taken advantage of.

2.3 Reconstruction

Using the models presented in previous sections, an algorithm can be built that reconstructs the distribution of media from the measured spectra. It is noticed that the 4 transverse resonance equations are minimized in the same manner regardless parameters. Since there are 4 equations at hand and 4 unknowns, it is suitable to apply Newton's method.

The full computational scheme consists of 2 steps, see figure 3 for result of the first step. First the resonance frequency and loaded quality factors are extracted for TE110 and TE210 modes. Typically, measured data is a transmission measurement - with weak coupling, the unloaded Q -factor can be approximated by the measured loaded Q - or otherwise, a more sophisticated transfer function that models coupling circuitry as well must be applied to obtain the unloaded Q and resonance frequency.

Using results of work [2] we can conclude that for resonance spectrum data with signal-to-noise ratio < 65 , a non-linear least squares fit to a Lorentzian curve is more accurate than fit to the phase vs. frequency. Thus, for a sufficiently weakly coupled resonator under test, where unloaded Q can be closer in value to the measured loaded Q , the transmitted resonance spectrum is anticipated to have more noise simply due to the relatively low signal level. One may then conclude that non-linear least squares fit to a Lorentzian curve is suitable for characterizing weakly coupled resonator configurations. We refer to [2] for review of different methods for calculating of resonance spectrum, extraction of Q -factor and resonance frequency.

The second step of our computational procedure is to use the measured Q -factors and resonant frequencies for TE110 and TE210 modes as input to a combined transverse resonance condition

for TE110 and TE210 modes, and solve then the equations using the optimization algorithm. In this work the Lorentzian function $L(\omega)$ is defined by the equalant circuit for the transverse resonator as shown in figure 4 and it is given by the formula

$$(20) \quad L(\omega) = A \cdot \left(\left(\frac{\omega_0}{2Q_0} \right)^2 \left((\omega - \omega_0)^2 + \left(\frac{\omega_0}{2Q_0} \right)^2 \right) \right) + B,$$

where $\omega = 2\pi f$ and $\omega_0 = 2\pi f_0$, f_0 is resonance frequency and Q_0 is quality factor, A is amplitude and B is constant. It is noticed that a realistic resonance curve has parasitic contributions from coupling circuitry, or parasitic parallel capacitance. Also, probes/antennas for resonance excitation may have intrinsic resonances which are "multiplied" to the resonance of interest.

It is noticed that a realistic resonance curve has parasitic contributions from coupling circuitry, or parasitic parallel capacitance. Also, probes/antennas for resonance excitation may have intrinsic resonances which are "multiplied" to the resonance of interest.

Typically, resonance frequency f_0 and quality-factor Q can be extracted by a simple peak search and a numerical direct extraction of the quality-factor from a ratio of band-width at half maximum peak value and resonance frequency. These extracted values are good initial guesses for f_{init}^{TE110} , Q_{init}^{TE110} and f_{init}^{TE210} , Q_{init}^{TE210} .

For one TE resonance, assuming that above conditions hold, we have four unknowns to be extracted: amplitude A_0^{TE110} , Q_0^{TE110} , f_0^{TE110} and B_0^{TE110} .

The same is valid for TE210 resonance. Only Q_0^{TE110} , f_0^{TE110} and Q_0^{TE210} , f_0^{TE210} are needed in order to extract the four unknowns liquid thickness, salinity, WLR and droplet ratio.

The measured quality factors Q_0^{TE110} and Q_0^{TE210} as well as the measured resonance frequencies f_0^{TE110} and f_0^{TE210} can be approximated to the unloaded corresponding entities as long as the coupling to the resonator is sufficiently weak - otherwise, the unloaded quality factors and resonant frequencies must be calculated by an analysis that includes the coupling circuitry influence. Here, for simplicity, we assume that the coupling is weak and that the unloaded and measured loaded entities are the same.

The reconstruction of the media content and distribution is solved by minimizing squared real and imaginary parts of transverse resonance functionals for TE110 and TE210:

$$(21) \quad \begin{aligned} J_W^{Re}(f_0^W, Q_0^W, x, K) &= \left(\text{Re} \left(Z_{in}(f_0^W, Q_0^W, x, K) + Z_{out}(f_0^W, Q_0^W, x, K) \right) \right)^2 = 0, \\ J_W^{Im}(f_0^W, Q_0^W, x, K) &= \left(\text{Im} \left(Z_{in}(f_0^W, Q_0^W, x, K) + Z_{out}(f_0^W, Q_0^W, x, K) \right) \right)^2 = 0 \end{aligned}$$

where W is TE110 or TE210 mode, x is the vector of 4 unknowns which are $x = (h, R_{WLR}, s, R_{DGR})$, and K is the static input parameters (temperature, pipe inner diameter and hydrocarbon permittivity).

Having four unknowns and four equations, Newton-Raphson method is suitable, since only first order derivatives needs to be calculated in a Jacobian matrix. One may add more sensors (the open ended coax resonator sensor shown in Fig. 2, for instance) so that an overdetermined non-linear system of equations is obtained. This overdetermined system may be reduced back to a set of 4 equations either by adding the sensor functionals $J_{quarter}$ (in eq. 22) to the existing 4 transverse resonance functionals. It is also possible to replace one of the existing transverse resonance functionals with the sensor functional $J_{quarter}$. To obtain 4 unknown parameters (h, R_{WLR}, s, R_{DGR}) we minimize the difference of the model value for reflection coefficient S_{11}^1 (in magnitude) and the magnitude of the measured reflection coefficient \tilde{S}_{11}^1 .

The measurement is taken exactly at the same point (reference plane) as the excitation (incident wave). A continuous wave in a certain frequency range is used, rather than a pulse. In addition to the 4 unknowns, the functional $J_{quarter}$ also depends on the geometric dimensions

and the dielectric media inside the pipe, in addition to the 4 unknowns. Thus, our goal is to minimize the following functional:

$$\begin{aligned}
(22) \quad J_{quarter}(h, R_{WLR}, s, R_{DGR}) = & \\
& \frac{1}{2} \int_{\omega_1}^{\omega_2} \left(|S_{11}^1(h, R_{WLR}, s, R_{DGR}, a, b, \omega')| - |\tilde{S}_{11}^1(\omega')| \right)^2 d\omega' \\
& + \frac{1}{2} \alpha_1 (h - h_0)^2 + \frac{1}{2} \alpha_2 (R_{WLR} - R_{WLR_0})^2 \\
& + \frac{1}{2} \alpha_3 (s - s_0)^2 + \frac{1}{2} \alpha_4 (R_{DGR} - R_{DGR_0})^2,
\end{aligned}$$

where $\alpha_j, j = 1, 2, 3, 4$ are small regularization parameters, such that $\alpha_j \in (0, 1)$. They can be chosen as constant values depending on the noise level δ , or iteratively using one of the iterative regularization algorithms, see [13, 14] for some of these algorithms. One of possible iterative choices for the computing of regularization parameters (see [14, 15] for computational details) is $\alpha_j^n = \alpha_j^0 (n+1)^{-p}$, where n is the number of iteration in any gradient-like method (in our case - number of iteration in Newton's method), $p \in (0, 1)$ and α_j^0 are initial guesses for $\alpha_j, j = 1, \dots, 4$. Similarly with [12] we choose $\alpha_j = \delta^\gamma$, where δ is the noise level and γ is a small number taken in the interval $(0, 1)$.

The expression (22) is in practice a sum due to the measured discrete frequency points ω_i with steps $\delta\omega'$:

$$\begin{aligned}
(23) \quad J_{quarter}(h, R_{WLR}, s, R_{DGR}) = & \\
& \sum_{i=0}^N \left(|S_{11}^1(h, R_{WLR}, s, R_{DGR}, a, b, \omega'_i)| - |\tilde{S}_{11}^1(\omega'_i)| \right)^2 \cdot \delta\omega' \\
& + \frac{1}{2} \alpha_1 (h - h_0)^2 + \frac{1}{2} \alpha_2 (R_{WLR} - R_{WLR_0})^2 \\
& + \frac{1}{2} \alpha_3 (s - s_0)^2 + \frac{1}{2} \alpha_4 (R_{DGR} - R_{DGR_0})^2.
\end{aligned}$$

The resulting functional for two identical open ended coax quarter-wave resonators - one capacitive and the second galvanic coupled - is:

$$\begin{aligned}
(24) \quad J_{quarter}(h, R_{WLR}, s, R_{DGR}) = & \\
& \sum_{i=0}^N \left(|S_{11}^{galv}(h, R_{WLR}, s, R_{DGR}, a, b, \omega'_i)| - |\tilde{S}_{11}^{galv}(\omega'_i)| \right)^2 \delta\omega' \\
& + \sum_{i=0}^N \left(|S_{11}^{cap}(h, R_{WLR}, s, R_{DGR}, a, b, \omega'_i)| - |\tilde{S}_{11}^{cap}(\omega'_i)| \right)^2 \delta\omega' \\
& + \frac{1}{2} \alpha_1 (h - h_0)^2 + \frac{1}{2} \alpha_2 (R_{WLR} - R_{WLR_0})^2 \\
& + \frac{1}{2} \alpha_3 (s - s_0)^2 + \frac{1}{2} \alpha_4 (R_{DGR} - R_{DGR_0})^2.
\end{aligned}$$

Mode	Relative Tunability	
	$h = 1mm$	$h = 2mm$
TE110	$3.701 \cdot 10^{-6}$	$5.107 \cdot 10^{-6}$
TE210	$7.452 \cdot 10^{-6}$	$1.293 \cdot 10^{-5}$
Quarter wave	$1.520 \cdot 10^{-5}$	$1.059 \cdot 10^{-5}$

Table 3: The table shows the relative frequency change, by adding $0.5\mu m$ to the liquid film thickness h . Considering the f_0 listed in table 4, these numbers represent frequency changes of the order $10^2 - 10^3$ Hz.

3 Results of simulation

A set of simulations with different salinities, DGR, WLR and liquid thickness h was performed. In all cases, initial guesses were set to the following:

$$\begin{aligned}
s_0 &:= s^{init} = s^{true} \cdot 1.3, \\
R_{DGR_0} &:= R_{DGR}^{init} = R_{DGR}^{true} \cdot 0.7, \\
R_{WLR_0} &:= R_{WLR}^{init} = R_{WLR}^{true} \cdot 0.7, \\
h_0 &:= R_h^{init} = h^{true} \cdot 1.3.
\end{aligned}$$

The frequency range for the open ended coax resonator pair was adapted in order to keep the resonance dips within a sufficiently wide frequency range. No noise was added to the synthetic “measured” data. The conclusion is that the open ended coax resonator pair have potential to significantly improve convergence and reduce the error (defined as $e = |x_{iterated} - x_{true}|/|x_{true}|$) by a factor of 100.

There is room for some optimization regarding the open ended coax resonator pair – for example the coupling capacitance value could be further optimized. Number of frequency points and frequency range are other details that may increase the benefits of having the open ended coax resonator pair. Also, for some combinations of salinity, WLR, DGR and liquid layer thickness, it may be more beneficial to only include either capacitive or galvanic coupled open ended coax resonator to increase convergence.

Regarding the coupling of the open ended coax resonator pair, it is noted that in the case of high salinity (typically salinity $> \sim 3\%$ for $R_{WLR} > 0.5$) one can obtain better salinity sensitivity from amplitude changes with the galvanic coupled resonator. This is demonstrated on Figures 10 and 11 where we choose liquid thickness $h = 4$ mm, and WLR=1, amplitude change versus salinity (for salinities from $4 \rightarrow 22\%$) is roughly a factor 2 larger for the galvanic coupled resonator compared to the capacitive coupled resonator. Thus, the sensitivity of amplitude will be typically a factor 2 larger for the galvanic coupled resonator except around the stagnation point at salinity $\sim 16\%$. Note that the sensitivity is depending somewhat on the coupling capacitance (in this work set to 10 pF).

If we look at “low” salinity regime (salinity $0 \rightarrow \sim 3\%$ for all WLR), the typical response of the capacitive coupled resonator is the one of a nearly critical coupled resonator with sharply defined skirts. The galvanic coupled resonator on the other hand, has a much less pronounced resonance dip (see figure 12 for simulation of reflection defined as reflected voltage/incident voltage). A change in liquid thickness or change in WLR would lead to a resonance frequency change and thus, the sensitivity of WLR or liquid thickness change is greater for the capacitive coupled resonator.

We denote the tunability as $\frac{f_0(h) - f_0(h + \delta h)}{f_0(h + \delta h)}$, where values of parameters are chosen as follows: $s = 10^{-7}$, $R_{DGR} = 0$, $R_{WLR} = 1$. In table 3 is shown the resonance frequency shift for a small liquid thickness change $\delta h = 0.5\mu m$. As seen in the table, the TE210 mode is shifted twice as much as the TE110 modes. This is as expected, since electrical field in TE210 mode is weaker in the center of the spool.

As seen in table 3, the tunabilities for TE modes and quarter wave coax are of the same order of magnitude, even though quarter-wave resonator tunability decreases with increased liquid layer h . It is the opposite for TE modes (at least in the h -range shown here).

Mode	Frequency, f_0 $h = 1mm$	Frequency, f_0 $h = 2mm$
TE110	1 041 453 582	1 032 491 153
TE210	1 717 407 914	1 684 125 223
Quarter wave, capacitive coupled	112 188 018	110 530 685

Table 4: The table shows the frequencies of the sensitivity analysed in table 3.

4 Discussion

We have presented a full wave transverse resonance model for a circular cylindrical annular geometry. It was demonstrated numerically that 4 unknown physical parameters could be extracted. If we combine the transverse resonance model with the reflection data from open ended quarter-wave resonators, we may improve convergence and reducing error by a factor of 100.

It was also demonstrated, that the combination of a galvanic and capacitive coupled open ended coax resonator renders higher sensitivity for WLR and liquid thickness. This is valid in low saline regime: salinity $< \sim 3\%$ for water continuous liquid case or for any salinity where $R_{WLR} < 0.5$.

This frequency sensitivity improvement is due to capacitive coupled open ended coax resonators sharper resonance pole skirts. For the high saline regime (water-continuous and salinity $> \sim 3\%$), better sensitivity (in amplitude change due to change in salinity) is obtained using the galvanic coupled coax resonator.

Acknowledgements

The authors are grateful for discussions with P.S. Kildal, Y. Yang, Z. Sipus, P. Slättman, H. Merkel and S. P. Hanserud.

References

- [1] A. Eriksson, A. Deleniv and S. Gevorgian, Orientation and direct current field dependent dielectric properties of bulk single crystal SrTiO₃ at microwave frequencies, *J. Appl. Phys.*, 2003, 93, pp. 2848
- [2] P.J. Petersan, S. M. Anlage, Measurement of Resonant Frequency and Quality Factor of Microwave Resonators: Comparison of Methods, *J. Appl. Phys.*, 1998, 84, pp. 339
- [3] A. Eriksson, P.Linner and S. Gevorgian, Mode chart of electrically thin parallel-plate circular resonators, *IEEE Proceedings-Microwaves Antennas and Propagation*, issue: 1, 2001, 148, pp. 51-55
- [4] A. Eriksson, A. Deleniv and S. Gevorgian, Resonant tunneling of microwave energy in thin film multilayer metal/dielectric structures, *Microwave Symposium Digest, 2002 IEEE MTT-S International*, 2002, 3
- [5] Roger F. Harrington, *Time-Harmonic Electromagnetic Fields*, Wiley-IEEE Press, 2001
- [6] L. Beilina, A. Eriksson, Reconstruction of dielectric constants in a cylindrical waveguide, *Springer Proceedings in Mathematics & Statistics, Inverse Problems and Applications*, 2015, 120, pp. 97-109

- [7] Z. Šipuš, P-S. Kildal, R. Leijon and M. Johansson, An Algorithm for Calculating Green's Functions of Planar, Circular Cylindrical, and Spherical Multilayer Substrates, *ACES Journal*, 1998, 13 (3)
- [8] D. H. Gadani et al., Effect of Salinity on the dielectric properties of water, *Indian Journal of Pure & Applied Physics*, 2012, 50, pp. 405-410
- [9] D. A. G. Bruggeman, Calculation of Various Physical Constants of Heterogeneous Substances, *Ann. Phys.*, 1935, 32 (12)
- [10] E. M. Kiley et al., Applicability Study of Classical and Contemporary Models for Effective Complex Permittivity of Metal Powders, *Journal of Microwave Power and Electromagnetic Energy*, 2012, 46, pp. 26-38
- [11] J. Baker-Jarvis et al., Analysis of an Open-Ended Coaxial Probe with Lift-Off for Nondestructing Testing, *IEEE Transactions on Instrument and Measurement*, 1994, 43 (5)
- [12] M. V. Klibanov, A. B. Bakushinsky, L. Beilina, Why a minimizer of the Tikhonov functional is closer to the exact solution than the first guess, *Journal of Inverse and Ill - Posed Problems*, 2011, 19, pp. 83-105
- [13] A. N. Tikhonov, A. V. Goncharsky, V. V. Stepanov and A. G. Yagola, *Numerical Methods for the Solution of Ill-Posed Problems*, London: Kluwer, 1995
- [14] A. Bakushinsky, M. Kokurin, A. Smirnova, *Iterative Methods for Ill-posed Problems*, De Gruyter, 2011, Inverse and Ill-Posed Problems Series 54
- [15] Samar Hosseinzadegan, Iteratively regularized adaptive finite element method for reconstruction of coefficients in Maxwell's system, *Master's thesis, Department of Mathematical Sciences, Chalmers, University of Gothenburg*, 2015

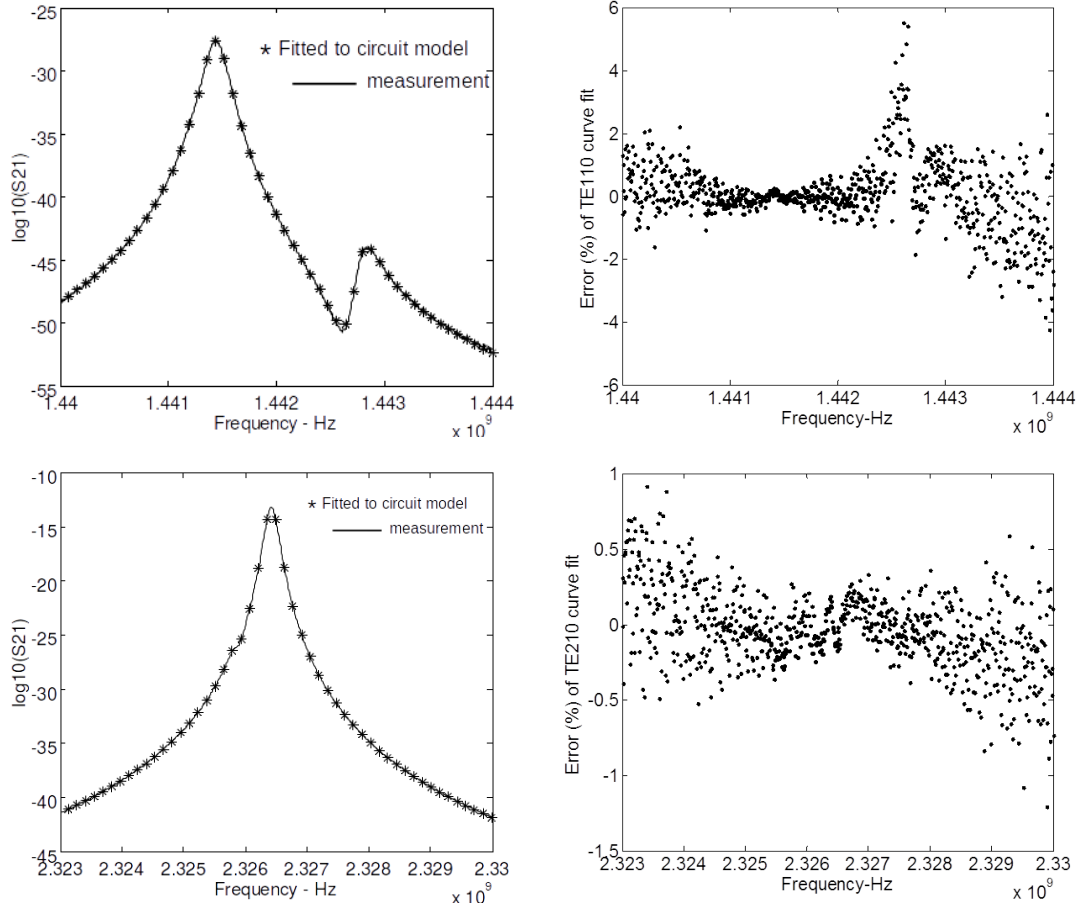


Figure 3: Result of step 1. Behavior of the Lorenzian function as a function of frequency, fitted to experimentally measured TE₁₁₀ (top figure) and a TE₂₁₀ (bottom figure) resonance in an air filled aluminium pipe of 128.5mm internal diameter. Resonant frequencies and quality factors are extracted from a Lorenzian fit the transmission measurement. Complex resonant frequencies are calculated as $f_0^{TE_{m10}} + i \frac{f_0^{TE_{m10}}}{2Q_0^{TE_{m10}}}$, which form input to the combined transverse resonant open ended coax functional. The figures on the right side show the relative difference between the measured data and the Lorenzian function.

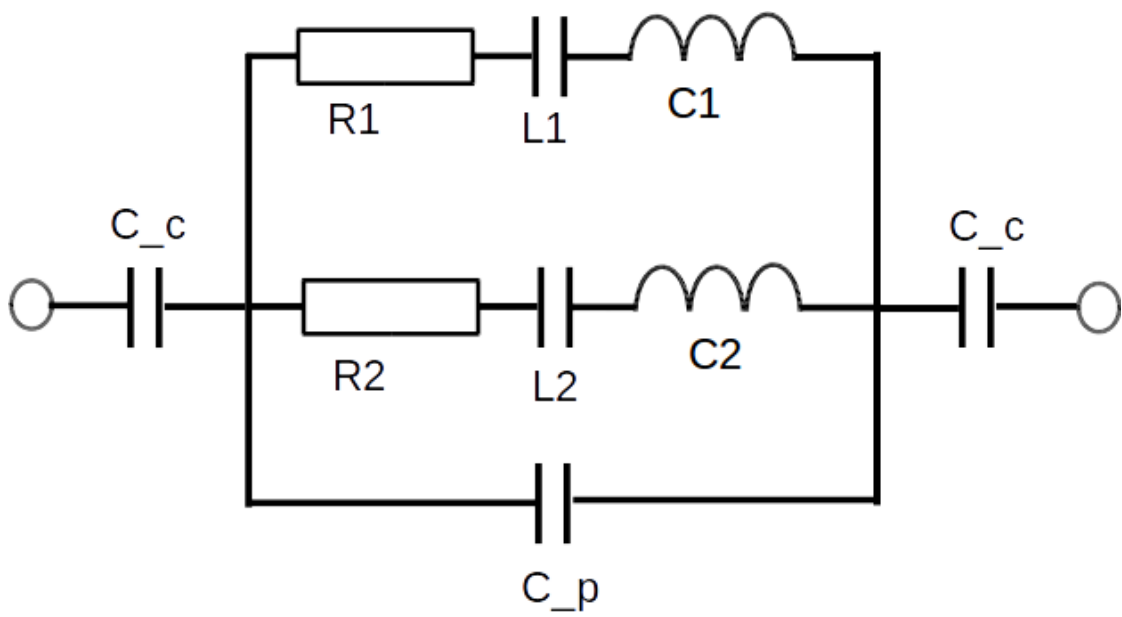


Figure 4: The diagram shows the equivalent electric circuit for the transverse resonator.

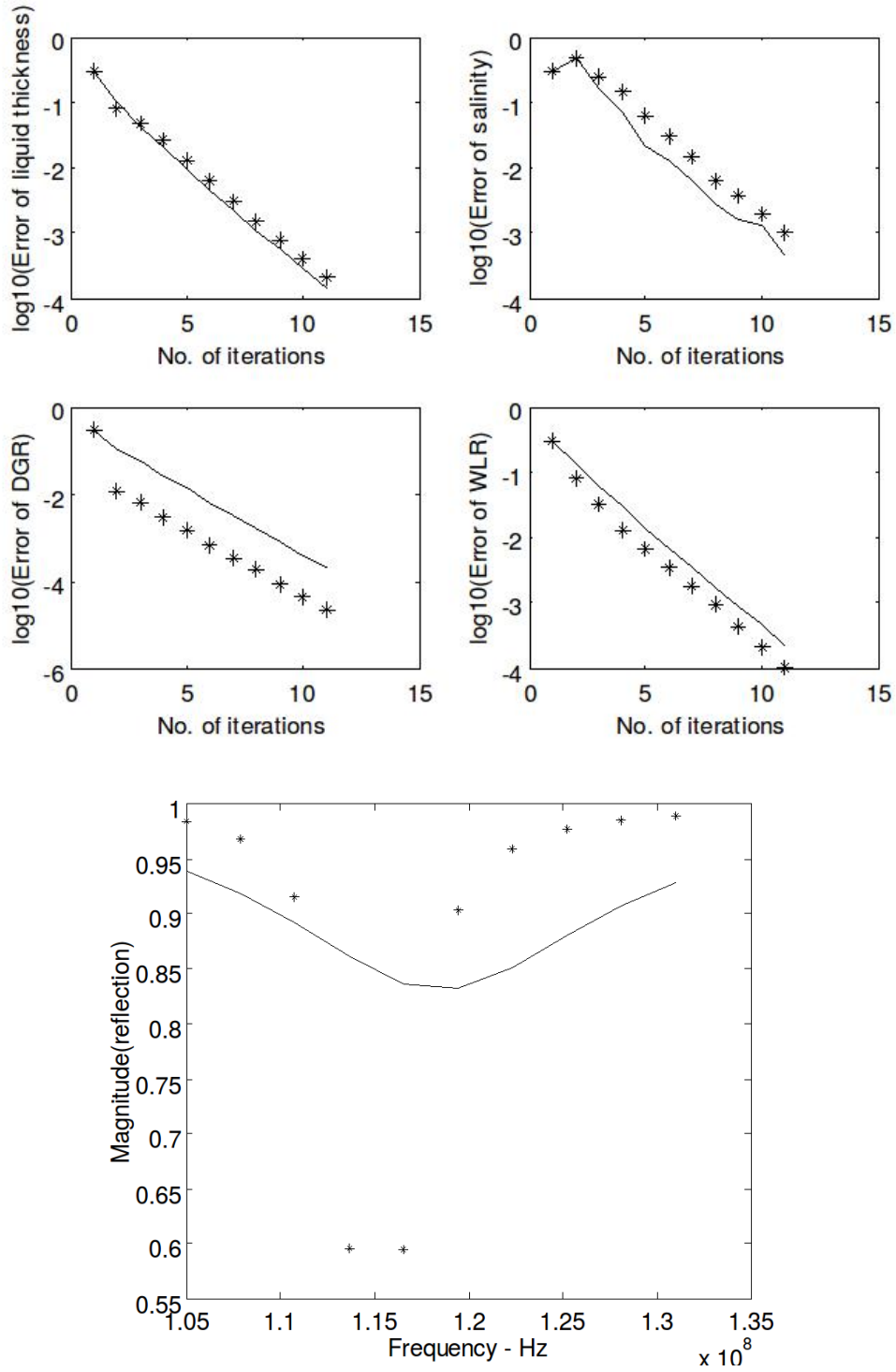


Figure 5: (Top) Error plots of simulation case for $s^{true} = 10^{-4}$, $h^{true} = 1\text{mm}$, $R_{DGR}^{true} = 10^{-2}$, $R_{WLR}^{true} = 0.1$. Solid line is without open ended quarter resonator pair. (Bottom) Magnitude of reflection of capacitive (+) and galvanic coupled (solid line) open ended coax resonators.

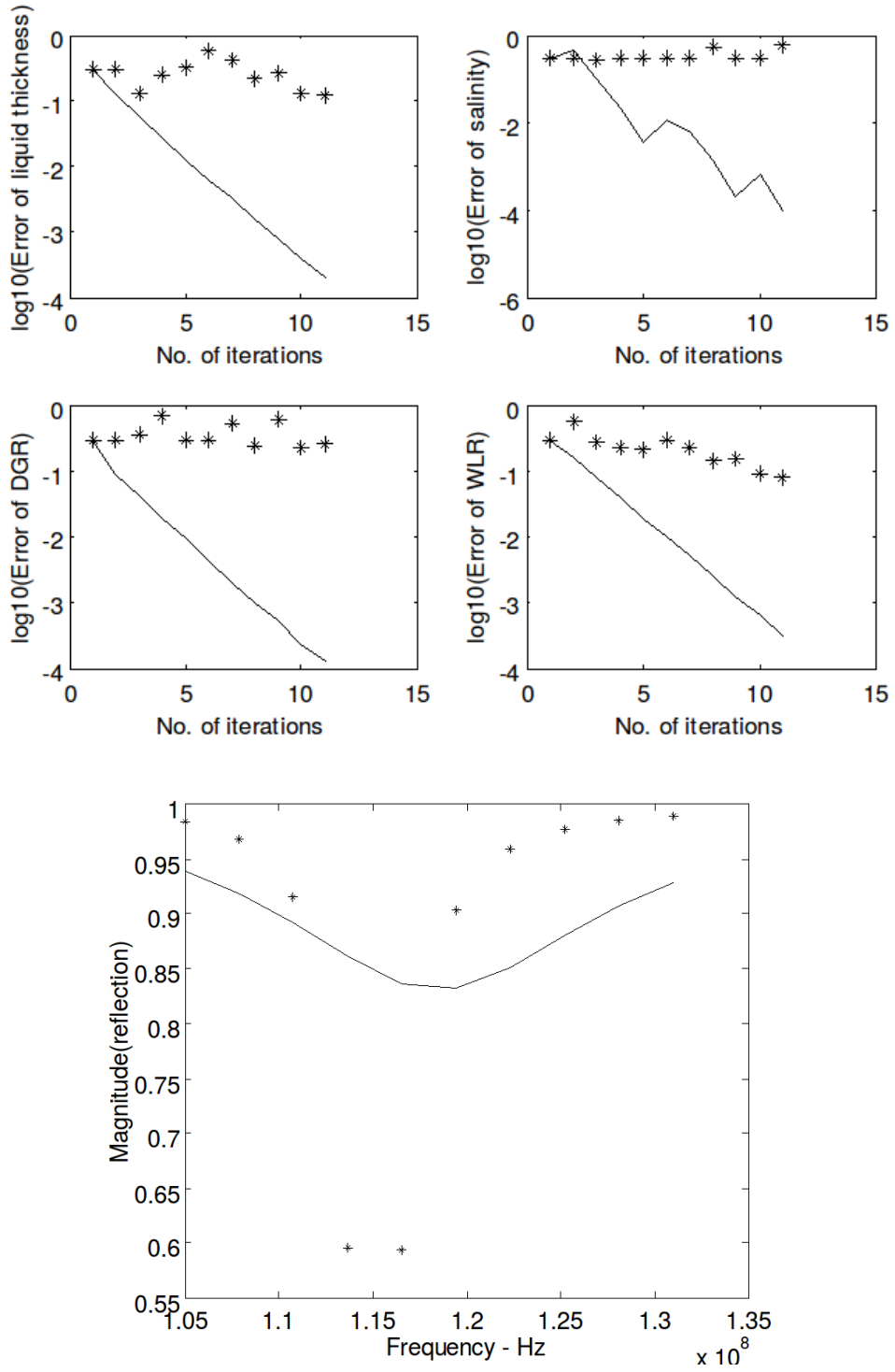


Figure 6: (Top) Error plots of simulation case for $s^{true} = 10^{-4}$, $h^{true} = 1\text{mm}$, $R_{DGR}^{true} = 2 \cdot 10^{-3}$, $R_{WLR}^{true} = 0.1$. Solid line is without open ended quarter resonator pair. (Bottom) Magnitude of reflection of capacitive (+) and galvanic coupled (solid line) open ended coax resonators.

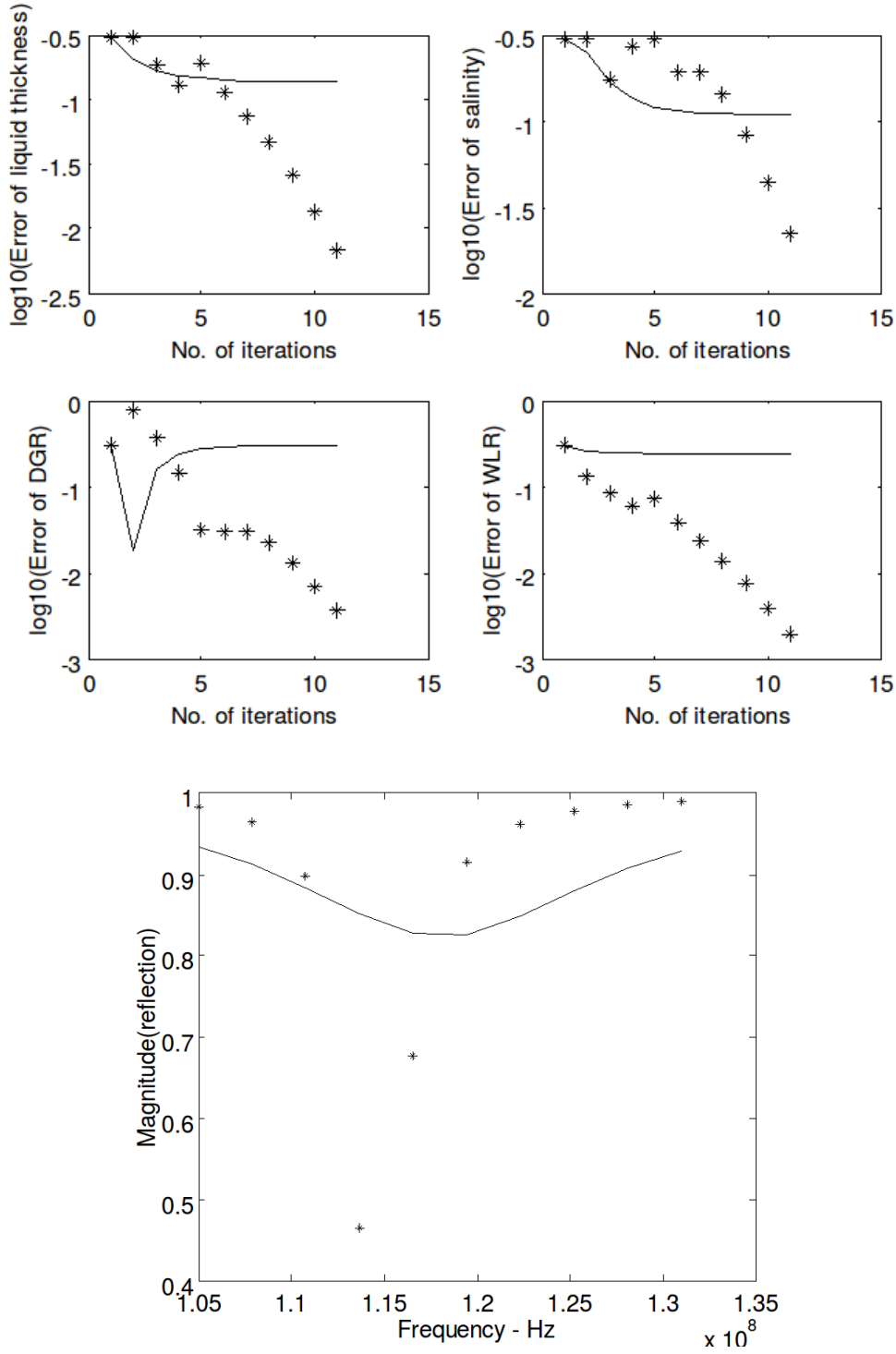


Figure 7: (Top) Error plots of simulation case for $s^{true} = 10^{-4}$, $h^{true} = 1\text{mm}$, $R_{DGR}^{true} = 10^{-2}$, $R_{WLR}^{true} = 0.4$. Solid line is without open ended quarter resonator pair. (Bottom) Magnitude of reflection of capacitive (+) and galvanic coupled (solid line) open ended coax resonators.

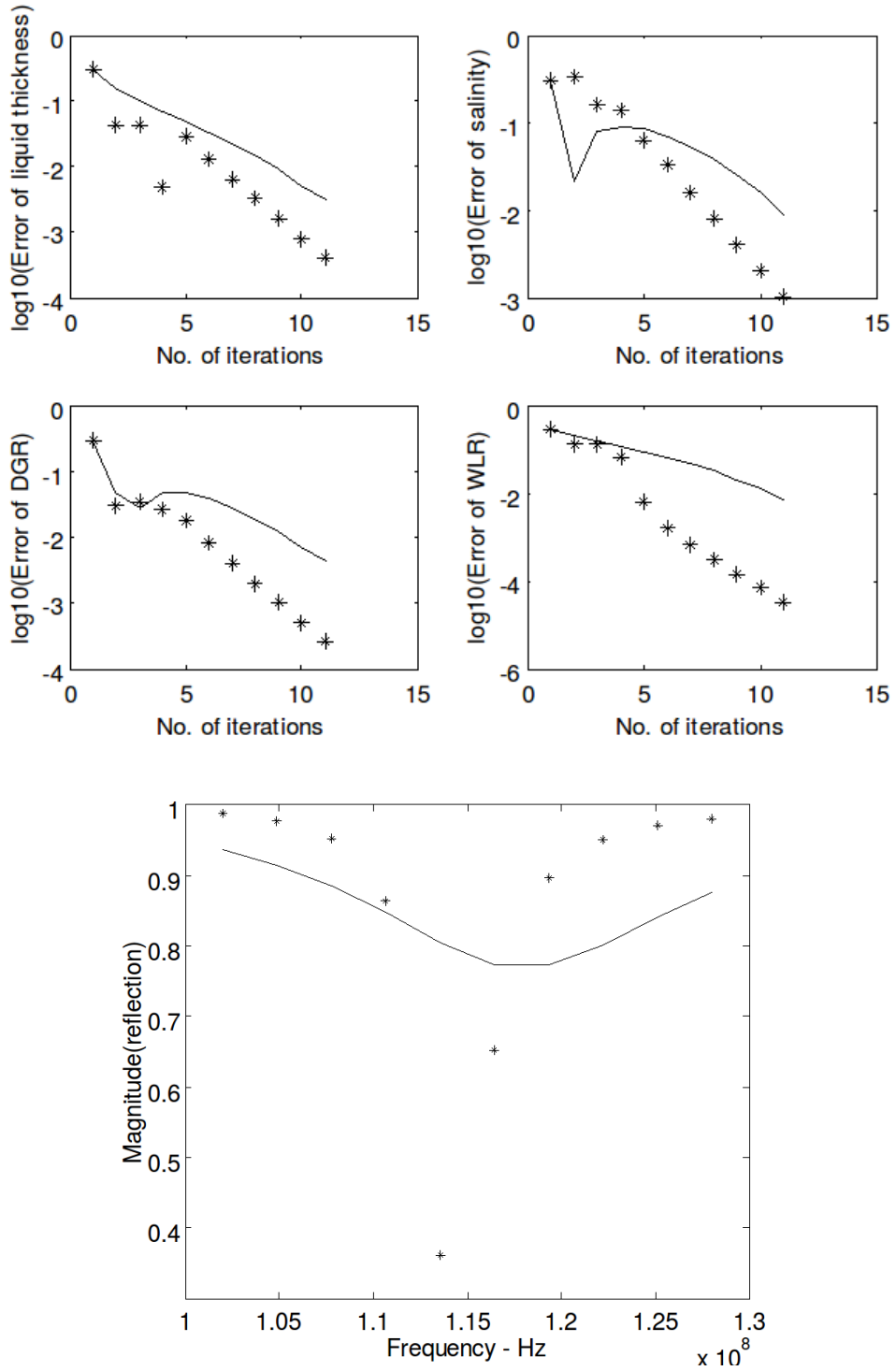


Figure 8: (Top) Error plots of simulation case for $s^{true} = 10^{-3}$, $h^{true} = 2\text{mm}$, $R_{DGR}^{true} = 10^{-2}$, $R_{WLR}^{true} = 0.4$. Solid line is without open ended quarter resonator pair. (Bottom) Magnitude of reflection of capacitive (+) and galvanic coupled (solid line) open ended coax resonators.

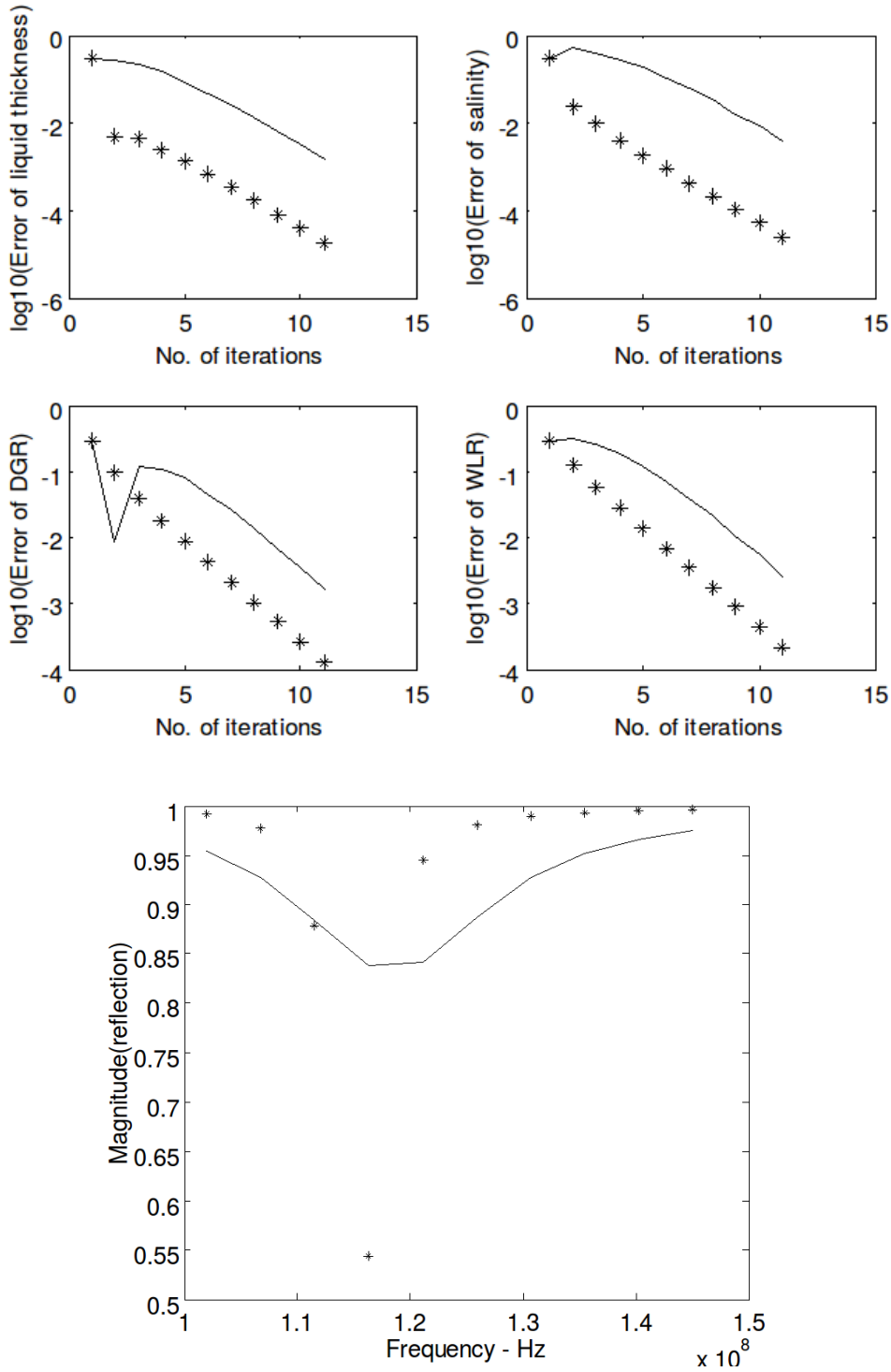


Figure 9: (Top) Error plots of simulation case for $s^{true} = 0.1$, $h^{true} = 2\text{mm}$, $R_{DGR}^{true} = 10^{-2}$, $R_{WLR}^{true} = 0.1$. Solid line is without open ended quarter resonator pair. (Bottom) Magnitude of reflection of capacitive (+) and galvanic coupled (solid line) open ended coax resonators.

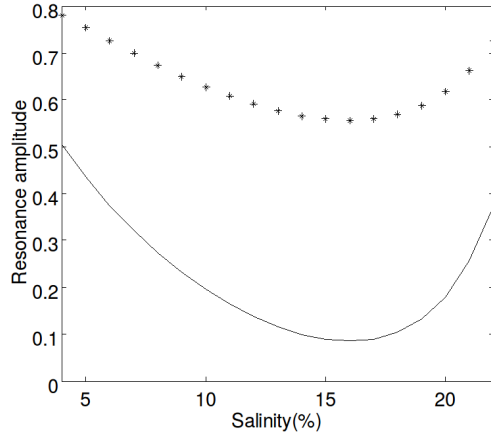


Figure 10: Comparison of amplitude for capacitive coupled (+) and galvanic coupled (solid line) open coax resonators at lowest resonance frequency versus salinity. Liquid thickness $h = 4mm$, $R_{WLR} = 1$ and $R_{DGR} = 10^{-5}$.

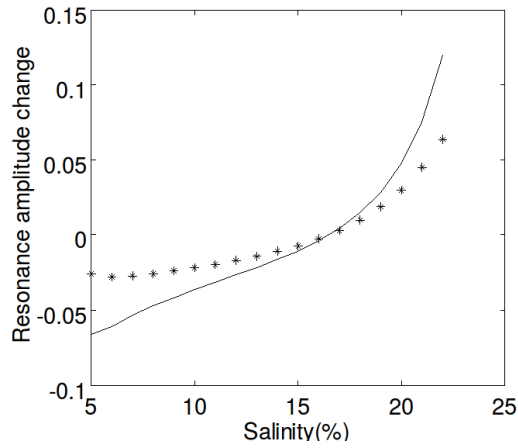


Figure 11: Comparison of amplitude change for capacitive coupled (+) and galvanic coupled (solid line) open coax resonators at lowest resonance frequency versus salinity. Liquid thickness $h = 4mm$, $R_{WLR} = 1$ and $R_{DGR} = 10^{-5}$.

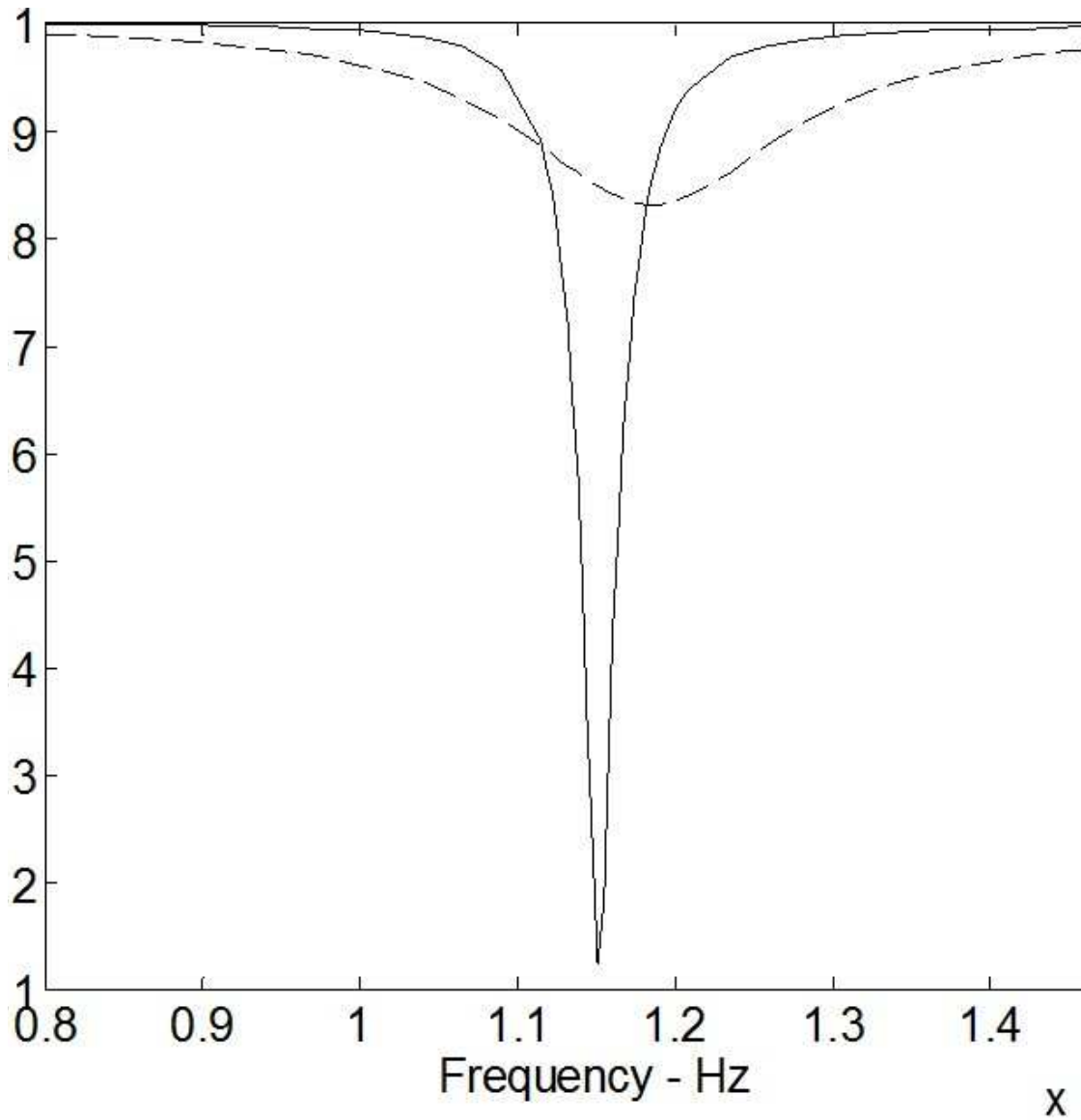


Figure 12: Simulation of reflection of capacitive coupled open coax resonator (solid line) and galvanic coupled open coax resonator (dashed line). $R_{WLR} = 10^{-3}$, $R_{DGR} = 10^{-2}$, $s = 10^{-3}$ and $h = 0$.